Carbon Nanostructure Examined by Lattice Fringe Analysis of High Resolution Transmission Electron Microscopy Images

Submitted to Environmental Science and Technology

Oct. 28th, 2002

Dr. Randy L. Vander Wal and Aaron J. Tomasek

The NCMR c/o NASA-Glenn

Dr. Kenneth Street and William K. Thompson

NASA-Glenn

Corresponding author:

Dr. Randy L. Vander Wal
NASA-Glenn
M.S. 110-3
21000 Brookpark Rd.
Cleveland OH 44135

Ph. 216-433-9065
Fax 216-433-3793
Email: randy@rvander.grc.nasa.gov

Abstract

The dimensions of graphitic layer planes directly affect the reactivity of soot towards oxidation and growth. Quantification of graphitic structure could be used to develop and test correlations between the soot nanostructure and its reactivity. Based upon transmission electron microscopy images, this paper provides a demonstration of the robustness of a fringe image analysis code for determining the level of graphitic structure within nanoscale carbon, i.e. soot. Results, in the form of histograms of graphitic layer plane lengths, are compared to their determination through Raman analysis.

Introduction

Although soot represents one of the very first nanostructured materials, it has rarely been considered as such. For decades, combustion research has focussed on its formation and growth. Early studies were heuristic, representing the diagnostic and computational tools available [1]. Later studies have provided detailed insights into its inception and growth from molecular species [2].

As found through both experimental and theoretical studies [3], in fuel-rich environments at elevated temperatures hydrocarbons undergo pyrolysis to produce mainly acetylene. As well described by the hydrogen abstraction, acetylene addition model, (the HACA mechanism) polycyclic aromatic hydrocarbons (PAHs) are formed by incremental C_2 addition to benzene [4]. Physical and reactive coagulation among these large PAHs results in soot precursor particles [5, 6]. More recent work has also shown the importance of dimerization among resonance stabilized radicals in producing high molecular mass PAHs [7]. Further mass addition by C_2H_2 and PAHs, along with carbonization results in soot [8, 9, 10]. Given the complexity and number of reaction steps in soot inception and growth; the effect upon soot internal structure has routinely been ignored.

When occasionally examined, soot internal structure has not been observed to differ substantially among laboratory-scale systems. This likely reflects the similarity of temperature and residence times in buoyancy-dominated flames [11, 12] and use of common hydrocarbon gases as fuels [13]. However, careful review of the general carbon literature does reveal that the structure of carbon materials is highly variable and is well known to depend upon the starting material and processing conditions. Carbons derived from different pitches have long been known to be either graphitizable or nongraphitizable [14]. Carbons produced from tars will have different degrees of

cross-linking, reflecting the structure of the starting material [15]. Chars derived from biomass fuels have a high degree of cross-linking that prevents their graphitization upon exposure to high temperatures [16]. Different coals are known to possess varying degrees of graphitizability [17-19]. Similarly, the nanostructure of carbon black also depends upon the reaction process [20].

The significance of the internal structure of carbon with respect to combustion is its effect upon reactivity. In general, more graphitic carbons are less reactive towards oxidation [21-27]. As a fundamental tenet in carbon science, a more graphitic carbon is characterized by layer planes with larger in-plane dimensions [17]. By virtue of geometry, larger layer planes contain fewer carbon atoms at edge sites relative to basal plane sites. The connection between layer plane dimensions and reactivity towards oxidation is due to the anisotropic reactivity of the graphitic segments comprising the carbon. Carbon atoms within basal plane sites, surrounded by other carbon atoms, exhibit a far lower reactivity towards oxidation than those located at the periphery of such segments (so-called edge sites) [21-27].

For these reasons, processes that induce growth of layer planes will necessarily affect the carbon's reactivity. For example, numerous examples of coal oxidation have found a decline of reactivity with increasing heat treatment [28-32]. Changes in the carbon nanostructure, such as an increase in graphitic layer plane length, have been correlated with this reactivity loss [30, 33]. This extension arises from a reorientation/reorganization of material. Layer plane segments can grow by bonding to adjacent graphene segments and by addition of amorphous carbon material within the soot particle [34-37]. Whether thermally or oxidatively induced, an increase in the dimensions of graphene segments corresponds to graphitization and a parallel decrease in reactivity.

High resolution transmission electron microscopy (HRTEM) can reveal the graphitic structure of carbon, i.e. its nanostructure. Such images provide a direct measure of the length,

2

shape and orientation of the graphitic fringes at any particular depth in the materials as determined by the focal plane [38]. As a measure of molecular order, quantification of the graphene segment dimensions could potentially be used to assess the reactivity of carbon towards oxidation. Correlations could then be developed between the extent of graphitic structure and oxidative reactivity, provided an algorithm to extract their size distribution from HRTEM images were available. Towards this goal this work sought to develop such an algorithm for soot.

Lattice fringe analysis has been employed to explain reactivity issues of other types of carbons. Shim et al. sought statistics on fringe length, tortuosity and other orientational order among graphene layers in solid fuel chars [39]. These authors sought to characterize the nanostructure as a function of residence time. This work was motivated by and built upon the observed decline in solid fuel char reactivity with increasing crystallinity. In related work, using HRTEM to examine the fine structure of chars, Zhang et al., identified a critical porosity as the factor determining fragmentation [40]. Moreover, the image analysis revealed an increase in order thereby accounting for the densification of the chars.

Prior to developing such correlations between structure and reactivity it is desirable to first test the robustness of the program for differentiating the varying levels of graphitic structure. To produce a reference set of soots with varying degrees of graphitic order, we applied thermal annealing to an amorphous grade of carbon black. As is well-known in carbon science, the final level of graphitic structure and organization will be dependent upon the combination of temperature and time at elevated temperature [41, 42]. For convenience with the instrumental apparatus available, we chose to vary the treatment temperature for a fixed time interval, as described next. The robustness of the algorithm for differentiating the degree of graphitic structure of these soots was then compared to Raman spectra as a traditional benchmark of graphitic materials.

3

Experimental

Samples of carbon black (Cabot R250 from Cabot Corporation) were heat-treated in a LECO EF-400 resistance heated furnace using a graphite crucible under a He atmosphere. The furnace was operated in power mode to maintain temperature stability and reproducibility. The temperature was inferred from factory provided calibration data. The heat treatment was a near trapezoid function of time with the temperature ramp up and cool down lasting less than 30 seconds with a soak time at elevated temperature of 10 minutes. An additional sample was obtained by inductive heating at 3000 ^{0}C for 1 hr. duration.

TEM images were taken using a Phillips CM200 with Gatan image filter (GIF) for digital imaging with live Fourier transforms having nominal resolution of 0.14 nm. The instrument operated at 200 keV using a LaB_6 filament. Gatan image software, v.3.4 was used for microscope operation. The real-space lattice fringe analysis program, as described later was based on Optimas v.6.5 with a custom windows-based macro interface, using the Gatan images as input.

A Renishaw Model 2000 Raman Microscope that uses a 25 mW Ar Ion laser operating at 514.5 nm was used to collect Raman spectra. Spectra were acquired in scan mode from 400-4000 cm^{-1} using an integration time typically between 10-50 seconds. The microscope objective employed was typically 20X with occasional spectra taken at 10X or 50X having spot diameters of 14, 28 and 5 microns respectively. The spectra presented here are single scans and are corrected for background. Spectra were taken from at least three areas of each sample to ensure that the spectra are representative of the material.

HRTEM Lattice Fringe Image Analysis

Using a fringe analysis program, the distribution of fringe lengths can be obtained. The

algorithm exists as a macro, running under Optimas version 6.5 [43]. Clearly any image analysis program needs input parameters to deal with the limitations in distinguishing fine features, adjacent objects, gray-scale levels and overall image contrast as determined by focussing variability. Therefore, this program features a menu driven interface for selection of the region of interest, correction for uneven illumination across the image (common in HRTEM imaging), spatial filtering prior to processing and a binary thresholding operation which extracts fringe areas from the background. The program also allows retouching to blank out any artifacts that lie within the region of interest that do not correspond to image data.

After the aforementioned image refinements, the user must input fringe parameters for the maximum join distance and minimum fringe length. The former parameter is used to repair fringes that have been bisected due to image artifacts or as a result of filtering or thresholding processes. Two fringe segments whose orientation angle is similar and whose endpoints lie within the N X N pixel neighborhood specified by this parameter will be joined and thereafter considered as one fringe. The purpose of the minimum fringe length is to discard any fringes whose length is less than this parameter. Execution of the macro utilizes these parameters to convert an image from grey-scale to binary. Carbon layer-plane thickness, which may increase with decreasing focus quality, is made constant at one pixel, creating a skeletonized, binary image. Non-physical conditions, such as sharp bends are also detected and separated. Among other outputs, the program displays the length of each fringe. A histogram is readily created from such data.

Results and Discussion

Figure 1 shows TEM images of the raw starting material, Cabot R250. With the outer graphene segments of the raw starting material being circumferential to the particle, they are properly aligned to anneal together. These outer shells or graphitic segments can then serve as templates for the less organized carbon within the particle interior, seen in Fig. 1a. Figure 2 shows

5

selected HRTEM images of the carbons subjected to different heat treatment temperatures of 1350, 1950, 2300 and 3000 °C, each representative of over 50 images. The growth in graphitic structure becomes markedly apparent with increasing thermal treatment. As observed for highly thermally annealed carbon blacks, the particles evolve towards faceted polygons with hollow interiors [44]. As seen, several parallel stacks of graphitic layer planes comprise each wall of the polygon. The net effect of increasing heat treatment temperature is to induce an increase in the number of stacked graphitic segments, improve their relative-alignment and in particular, extend their length. The focus here is on the latter quantity, as it pertains directly to the anisotropic reactivity of carbon.

Figure 3 shows the skeletonized images corresponding to each HRTEM image shown in Fig. 2. The image processing operations described above have been applied to the raw image data to obtain these processed images. As observed, these images display high similarity to the length and orientation of lattice fringes seen in the HRTEM input images. This visual comparison qualitatively verifies the processing fiduciary relative to the HRTEM data. These binary images show a clear increase in fringe length across the series of annealed carbon blacks. Individual fringe lengths were abstracted from these images and the subsequent distributions are summarized in the histograms presented in Fig. 4. With increasing heat treatment temperature, the relative percentage of short fringes declines while that of longer fringes increases. This increase is attributed to both joining of adjacent fringes, where their mobility is aided by the elevated temperature, and addition of adjacent random and disordered carbon to lamella. We note that for these samples, tortuosity and relative orientation of parallel graphitic segments are not highly variable and consequently will not be pursued further here.

Raman Comparison

Image fringe analysis provides a non-integrated, direct measure of the soot nanostructure. Relative to traditional measures of graphitic structure such as Raman spectroscopy, it offers three

advantages. First, image fringe analysis provides a detailed measure of the graphitic structure as described by the distribution of graphene segment lengths. Additional capabilities include tortuosity and curvature, to be discussed elsewhere. Second, based on HRTEM, it can provide spatially resolved measures of variations in lattice fringe structure within carbon structures. Third, it can be applied to vanishingly small (nanogram) samples. Nevertheless, it is instructive to compare the fringe analysis results with those provided by Raman for comparison of the fringe length data, i.e. relative graphitic content.

Raman spectroscopy has been tested as a method for determining the planar crystallite dimensions of carbons that possess limited long-range order [45]. Several measures have been applied to the spectra that have been correlated with the extent of graphitic structure, such as line-width, peak positions and peak intensity ratios [46]. Two spectral peaks characterize the first order Raman spectra of carbon materials; a very strong, high-frequency, in-plane stretching mode (E_{2g} or "G" peak near 1580 cm-1) and a weaker, low-frequency mode (A_{1g} or "D" peak near 1360 cm-1) [47]. The former corresponds to an in-plane stretching motion of the graphitic layer planes while the latter arises from a breakdown of the Raman selection rules attributed to the finite-sized regions of graphitic structure. Hence its nomenclature as the "disorder activated" transition.

The intensity ratio of these peaks has been interpreted as a measure of the in-plane crystallite dimensions [45]. Strong monotonic correlations have been shown between the D/G intensity ratio and heat treatment temperature [48, 49]. The most consistent semi-empirical relation to be developed is that by Knight and White, who found the in-plane crystallite dimension, L_a, to be an approximately linear function of the ratio of the integrated spectral peak intensities, (I_D/I_G) as applied to a wide range of carbon materials including pyrolytic, glassy, amorphous and crystalline graphite [45]. This relationship is particularly appealing as it affords a direct comparison with the

7

graphitic fringe length as provided by the fringe analysis program. The Raman spectra of the

different heat-treated carbon black samples are plotted in Fig. 5. The change in relative intensities

is consistent with increasing graphitization induced by higher temperatures. The narrowing of the

D and G peaks indicates increasing homogeneity of the sample as disordered carbon is reorganized

and/or joins to growing lamella.

Figure 6 shows graphs of the integrated intensity ratio of the G and D peaks of the carbon

nano-onions as a function of the heat treatment temperature. Plotted for comparison are the

medians of the fringe length histograms shown in Fig. 4 corresponding to the selected heat

treatment temperatures. Particularly encouraging is the monotonic relation exhibited by both the

Raman integrated intensity ratio and lattice fringe length with increasing temperature. In fact, each

best fit line possess a rather similar slope, as seen in Fig. 6. The monotonic behavior confirms the

dependence of each measure upon graphitic structure. The linear behavior common to each

quantity validates their self consistency of each as a gauge of the soot nanostructure.

As noted, peak intensities from Raman spectroscopy, when applied to disordered carbon

materials possessing very small domains of graphitic structure, are affected by layer plane

curvature, degree of turbostratic stacking, etc [50]. Additionally, we note that the lattice fringe

lengths observed using HRTEM are averaged over the viewing angle and hence any anisotropy in

the dimensions of the lamella will be subject to an angle-dependent length reduction within the

image. (However this factor would be consistent between HRTEM images of different carbon

nanostructures, thus relative values would be accurate.) Therein we refrain from using a

multiplicative semi-empirical factor to convert the Raman intensity ratios into fringe length or vice

versa. Rather, each method provides a different relative measure of fringe length. Nevertheless,

the approximate agreement and clear monotonic correlation supports the fringe analysis program as

providing an accurate measure of the graphitic structure, and hence potential oxidation

characteristics of the carbon.

In conclusion, a lattice fringe analysis program has been developed to quantify the data conveyed by HRTEM images. By providing a direct measure of the molecular level of graphitic structure, it is expected that its application could provide predictive capabilities for carbon reactivity, particularly towards oxidation. The robustness of this program is demonstrated by using a series of carbon blacks possessing different levels of graphitic structure, prepared at different heat treatment temperatures. Its credibility is benchmarked against a traditional measure of graphitic structure, as provided by Raman analysis. Lattice fringe length is found to be monotonic with the level of graphitic structure as provided by the ratio of the integrated intensities of the G/D spectral peaks in the Raman spectra. Reciprocally, for production purposes, the G/D band intensity ratio can serve as a direct measure of the lattice fringe reactivity.

Acknowledgements

Disclaimer

Trade names or manufacturers' names are used for identification only. This usage does not constitute an official endorsement, either expressed or implied by either the National Aeronautics and Space Administration or The National Center for Microgravity Research.

References

1. Gaydon, A. G., and Wolfhard, H. G., Flames, Their Structure, Radiation and Temperature, 3rd. Ed. Chapman and Hall, London, **1970**.

2. Physical and Chemical Aspects of Combustion, A tribute to Irvin Glassman, (F. L. Dryer and R. F. Sawyer, Eds.) Gordon and Breach Science Publishers, **1997**. pp. 107-266.

3. Proceedings of the International Workshp on Mechanisms and Models of Soot Formation (H. Bockhorn Ed.) Springer-Verlag, Heidelberg Germany, **1994**.

4. Frenklach, M. and Wang, H., Twenty-Third Symposium (International) on Combustion, The Combustion Institute **1990**, p. 1559.

5. Miller, J. H., Twenty-Third Symposium (International) on Combustion, The Combustion Institute, Pittsburgh PA **1990**, pp. 91-102.

6. Howard, J. B., Twenty-Third Symposium (International) on Combustion, The Combustion Institute, Pittsburgh, **1990**, p. 1107-1121.

7. Hepp, H., Siegmann, K. and Sattler, K., *Chem. Phys. Lett.* **1995**, 233, 16.

8. Xu, F., Lin, K.-C. And Faeth, G. M., *Comb. and Flame* **1998**, 115, 195.

9. Kronholm, D. F., and Howard, J. B., The Twenty-Eighth Symposium (International) on Combustion, The Combustion Institute, Pittsburgh PA **2000**, pp. 2555-2561.

10.) R. A. Dobbins, R. A. Fletcher, and W. Lu, "Laser microprobe analysis of soot precursor particles and carbonaceous soot", *Combust. and Flame* **1995**, 100, 301.

11. Law, C. K. and Faeth, G. M., Prog. *Energy Combust. Sci.* **1994**, 20, 64.

12. Santoro, R. J., Yeh, T. T., Horvath, J. J. and Semerjian, H. G., *Combust. Sci. and Tech.* **1987**, 53, 89.

13. Glassman, I., The Twenty-Second Symposium (International) on Combustion, The Combustion Institute, Pittsburgh PA **1988**, pp. 295-311.

14. Oberlin, A., *Carbon* **1984**, 22, 521.

15. Lewis, I. C., *Carbon* **1982**, 20, 519.

16. Wornat, M. J., Hurt, R. H., Yang, N. Y. C., and Headley, T. J., *Combust. and Flame* **1995**, 100, 131.

17. Wilks, K. R., Mastalerz, M., Bustin, R. M. and Ross, J. V., *Int. J. of Coal Geology* **1993**, 22, 247.

18. Buseck, P. R., Go-Jun, H. and Keller, L. P., Energy and Fuels **1987**, 1, 105.

19. Suuberg, E. M., Wojtowicz, M. and Calo, J. M., *Carbon* **1989**, 27, 431.

20. *Carbon Black Science and Technology*, 2nd ed. J. B. Donnet, R. C. Bansal and M.-J. Wang eds. Marcel Dekker, Inc.**1993**.

21. Smith, W. R. and Polley, M. H., *J. Chem. Phys.* **1956**, p. 689.

22. Thomas, J. M., Microscopy studies of graphite oxidation, in The Chemistry and Physics of Carbon, (P. L. Walker, Jr., Ed.) **1965**, Vol. 1, Chp. 2.

23. Henning, G. R., Chemistry and Physics of Carbon, (P. L. Walker, Jr., Ed.), **1966**, Vol. 2, Chp. 1

24. Levy, M., and Wong, P., *J. of The Electrochem. Soc.* **1964**, 11, 1088.

25. Rosner, D. E. and Allendorf, H. D., *AIAA Journal* **1968**, 6, 650.

26. Donnet, J. B., *Carbon* **1982**, 20, 267.

27. Marsh, H., Introduction to Carbon Science, Butterworths, London, **1989**, Chp. 4, pp. 107.

28. Smith, O. I., *Prog. Energy Combust. Sci.* **1981**, 7, 275.

29. Hurt, R. H., Dudek, D. R., Longwell, J. P. and Sarofim, A. F., *Carbon* **1988**, 26, 433.

30. Hurt, R. H., Sarofim, A. F. and Longwell, J. P., *Combust. and Flame* **1993**, 95, 430.

31. Fletcher, T. H., Ma, J., Rigby, J. R., Brown, A. L. and Webb, B. W., *Prog. Energy Combust. Sci.* **1997**, 23, 283.

32. Hurt, R. A., The Twenty Eighth Symposium (International) on Combustion, The Combustion Institute, Pittsburgh, PA **1998**, pp. 2887-2904.

33. Davis, K. A., Hurt, R. H., Yang, N. Y., and Headley, T. J., *Combust. and Flame* **1995**, 100, 31.
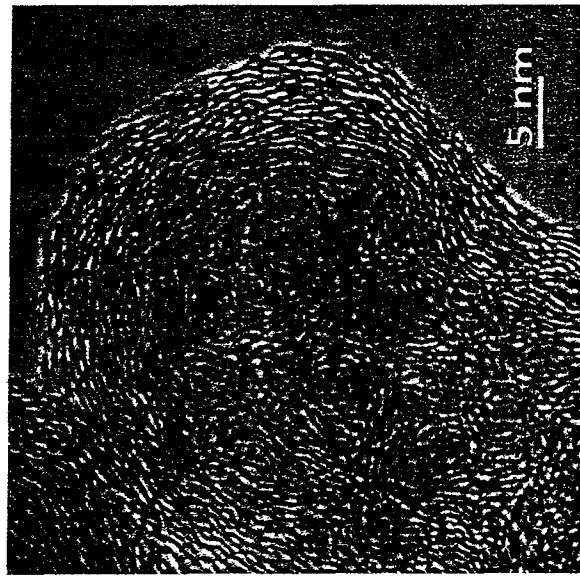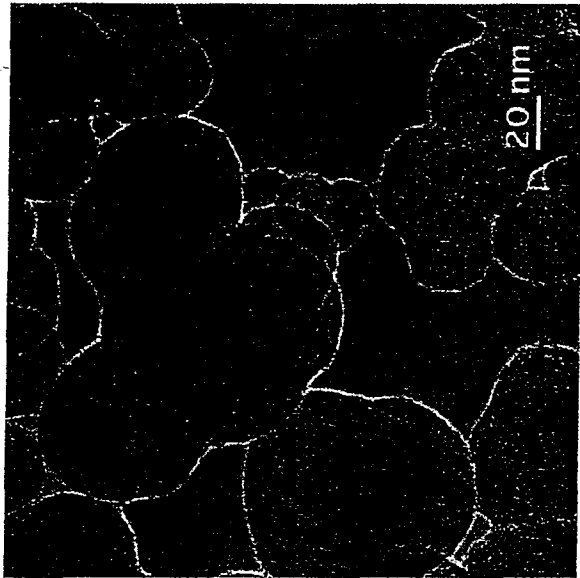
34. Heckman, F. A. and Harling, D. F., *Rubber Chem. and Technol.* **1966**, 39, 1. See also The Presentation at the Annual meeting of the Division of Rubber Chemistry, The American Chem. Soc., Miami Beach,

35. Hess, W. M., Ban, L. L., Eckert, F. J. and Chirico, V. *Rubber Chem. and Technol.* **1968**, 41, 356.

36. Marsh, P. A., Voet, A., Mullens, T. J. and Price, L. D., *Rubber Chem. and Technol.* **1970**, 43, 470.

37. Vander Wal, R. L., and Choi, M. Y., *Carbon* **1999**, 37, 231.

38. Vander Wal, R. L., *Combust. Sci. and Technol.* **1997**, 126, 333.

39. Shim, H.-S., Hurt, R. H. and Yang, N. Y. C., *Carbon* **2000**, 38, 29.

40. Dukhan, X. Z., Kantorovich, I. I., Bar-Ziv, E., Kandas, A., and Sarofim, A. F., Twenty-Sixth Symposium (International) on Combustion, The Combustion Institute, Pittsburgh, PA **1996**, pp. 3111-3118.

41. Akamatu, H., and Kuroda, H., Proc. 4th Carbon Conference, Pergamon Press Inc., New York **1960**, pp. 355.

42. Emmerich, F. G., *Carbon* **1995**, 33, 1709.

43. Optimas, Media Cybernetics L.P., Siver Springs, MD.

44. Millward, G. R., and Jefferson, D. A., Lattice resolution of carbons by electron microscopy, in "The Chemistry and Physics of Carbon", Vol. 14, (P. L. Walker and P. A. Thrower, Eds.), Marcel Dekker Inc., New York, **1970**, Chp. 1.

45. Knight, D. S., and White, W. B., *J. Mater. Sci.* **1989**, 4, 385.

46. Fischbach, D. B., and Couzi, M., *Carbon* **1986**, 24, 365. (and references therein).

47. Tuinstra, E., and Koenig, J., *J. Chem. Phys.* **1970**, 53, 1126.

48. Nakamizo, M., Kammereck, R., and Walker, Jr., P. L., *Carbon* 1974, 12, 259.

49. Emmerich, F. G., *Carbon* **1995**, 33, 1709.

50. Dresselhaus, M. S., Dresselhaus, G., Sugihara, K., Spain, I. L., and Goldberg, H. A., Graphite Fibers and Filaments, Springer-Verlag, Heidelberg Germany **1988**, Chp. 4, pp. 97.

Figure Captions

Figure 1   TEM images of the raw material (carbon black) used for producing the graphitized carbon by heat treatment. The material product designation is Cabot R250.

Figure 2   High resolution transmission electron microscopy images of the carbon black prepared by heat treatment at temperatures of a) 1350, b) 1950, c) 2300 and d) 3000 °C

Figure 3   Skeletonized images obtained by applying the lattice fringe analysis program to the HRTEM images shown in Fig. 2 of the carbon black soot processed at the different elevated temperatures.

Figure 4   Histograms of the lattice fringe lengths observed spatially in the binary processed images shown in Fig. 3. See text for details.

Figure 5   Raman intensity plots (1st order spectra) for the carbon black subjected to the different heat treatment temperatures.

Figure 6   Plots of the mean lattice fringe lengths obtained from histograms in Fig. 4 and the ratios of the integrated intensities of the Raman G and D spectral peaks (I_g/I_d) obtained from Fig. 5.

Fig. 1

Unheated Carbon Black
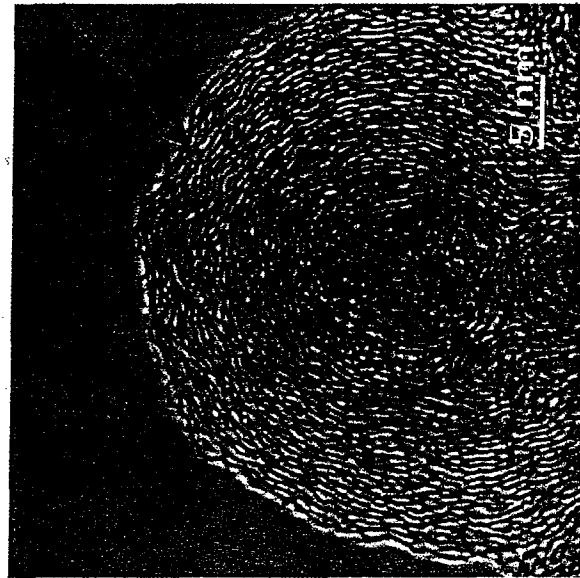
Graphene Segments
(tangential dark lines)

Fig. 2

Heat Treated Carbon Black

Exterior

Interior

1950 °C

5 nm

3000 °C

5 nm

1350 °C

5 nm

2300 °C

5 nm
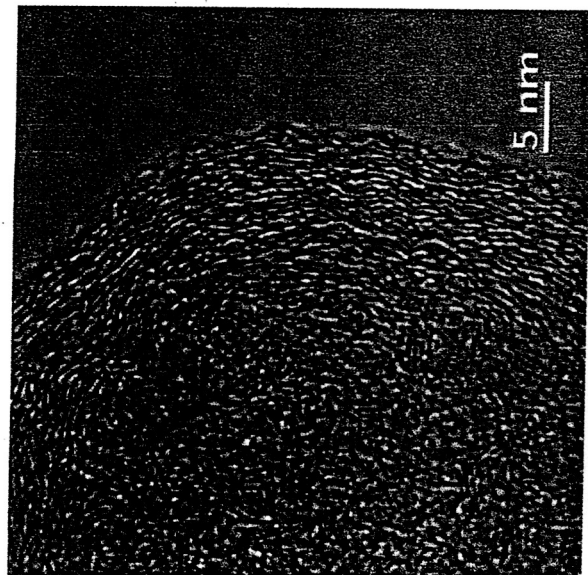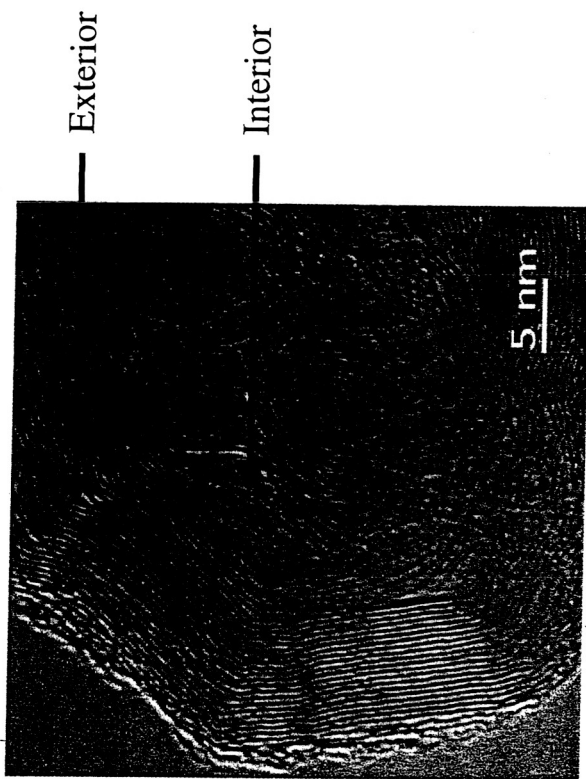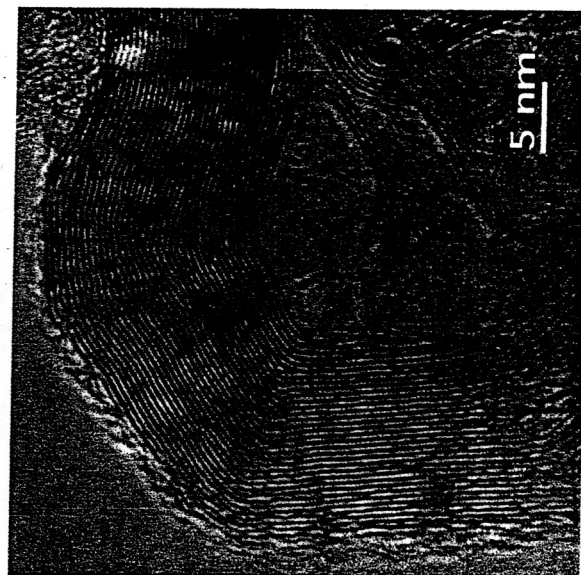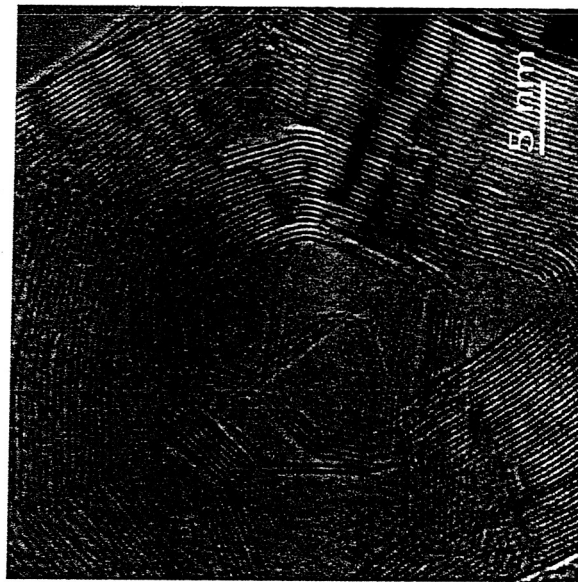
Fig. 3
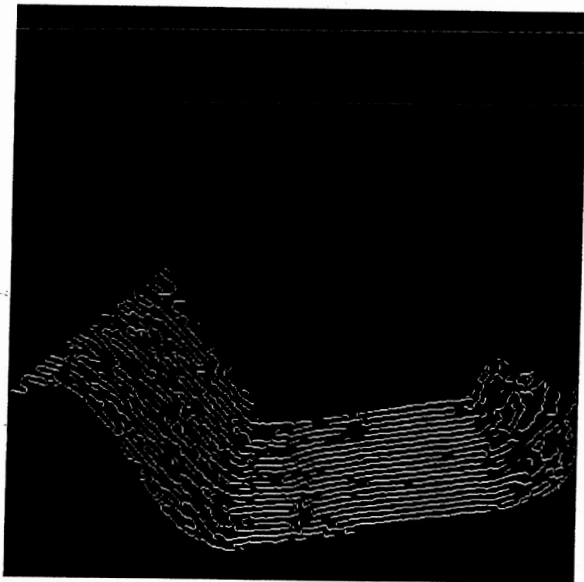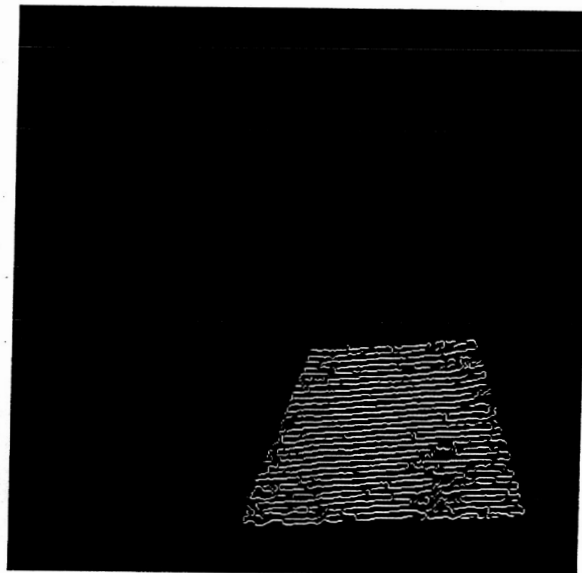
Skeletonized Images

1350 °C

1950 °C

2300 °C

3000 °C

Fig. 4

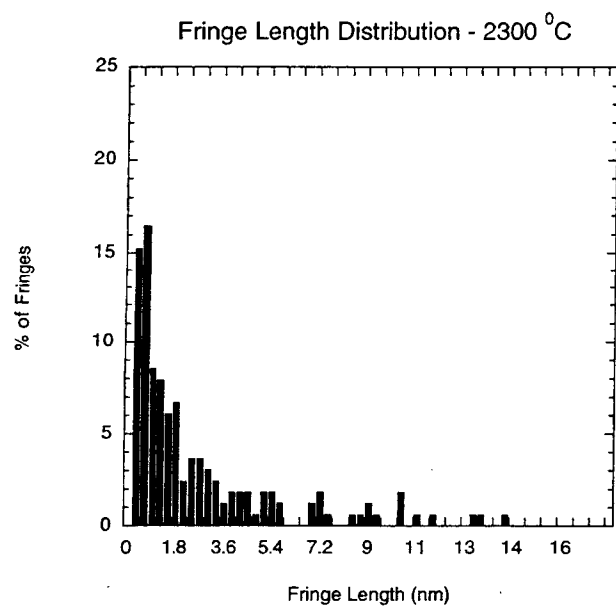Fringe Length Distribution - 1350 °C

Fringe Length Distribution - 1950 °C

Fringe Length Distribution - 2300 °C

Fringe Length Distribution - 3000 °C
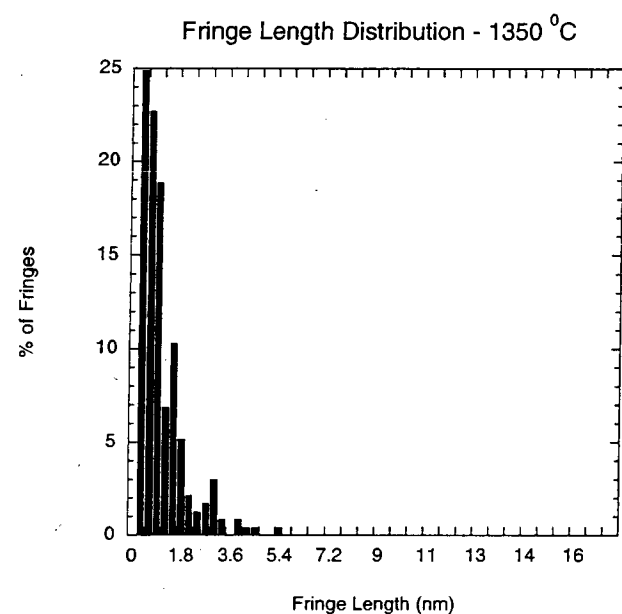
Fig. 5

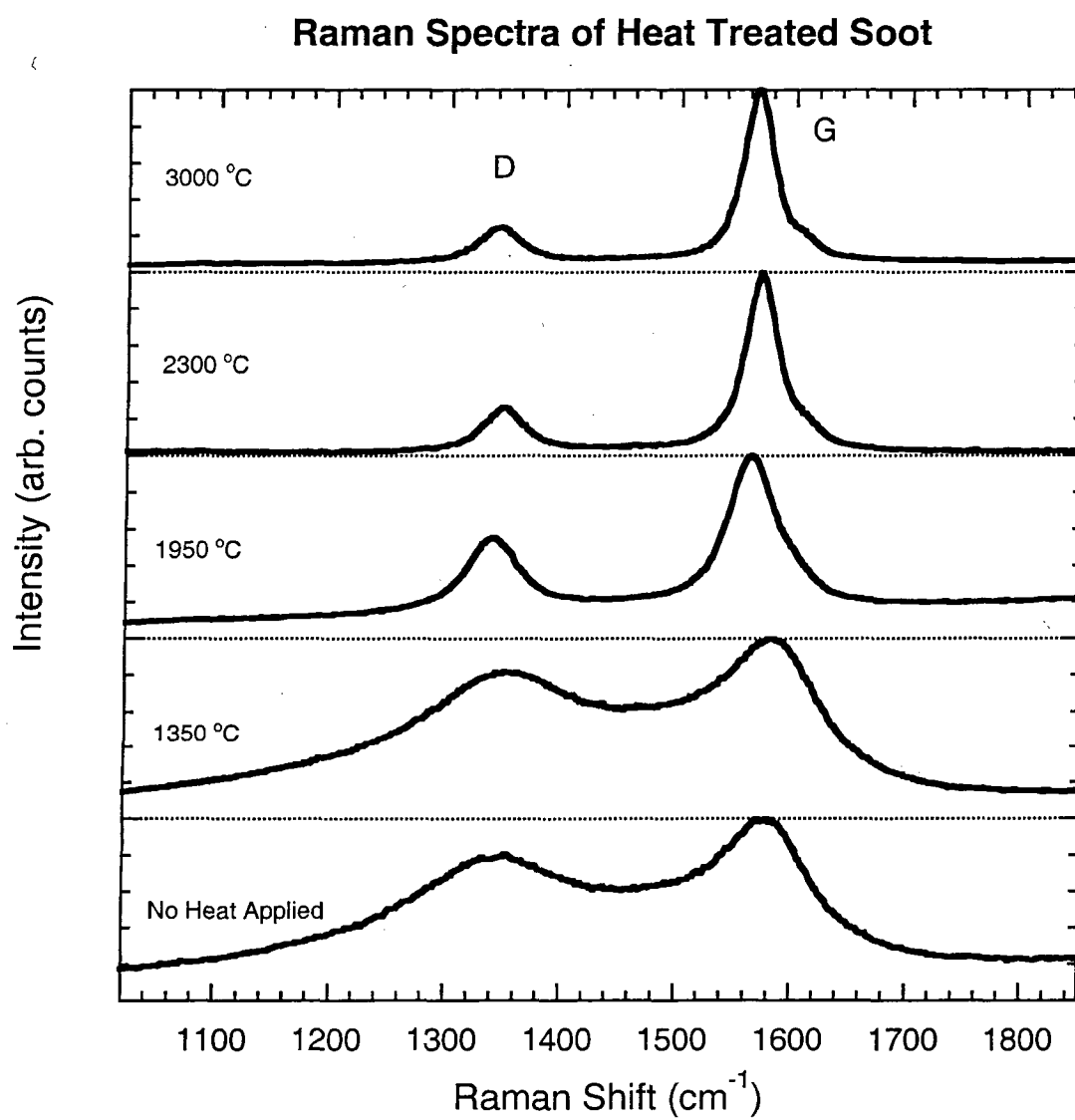Raman Spectra of Heat Treated Soot
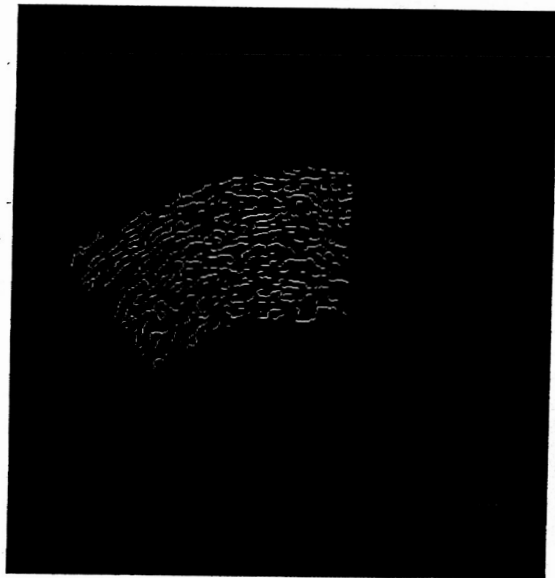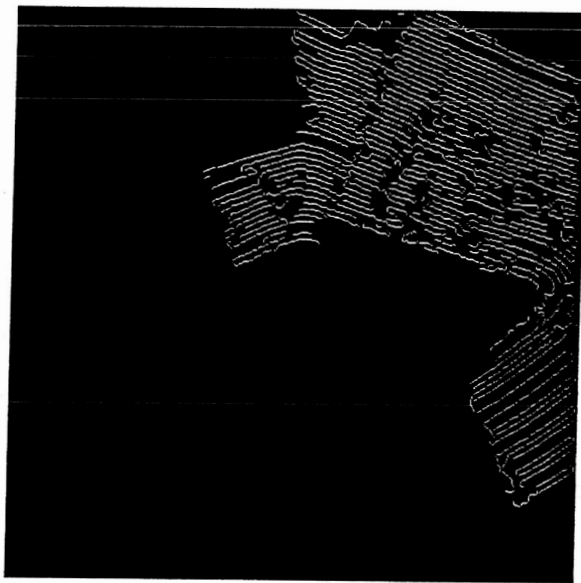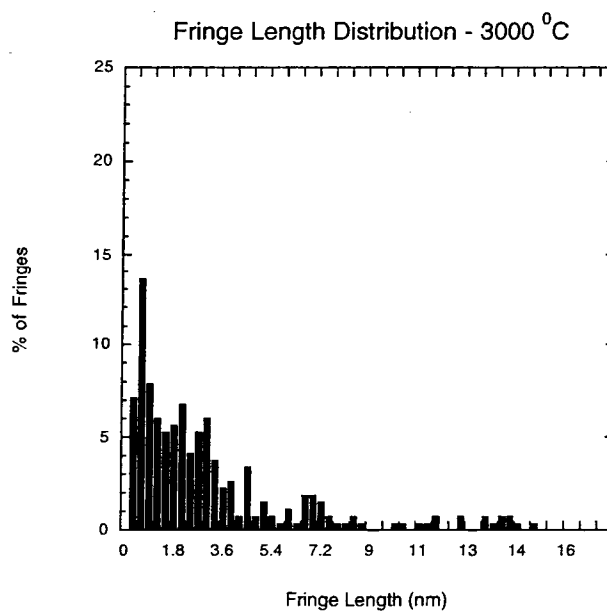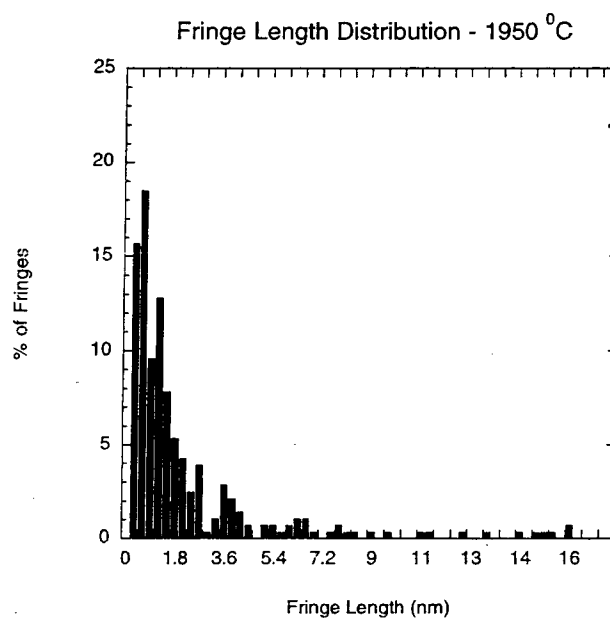
Fig. 6

Ratios of Integrated Raman Intensities for Heat Treated Carbon Blacks